MICROSEGREGATION IN DIRECTIONALLY SOLIDIFIED Ni-BASED SUPERALLOY

MILAN FLORIAN

Structure and microsegregation was studied in directionally solidified Ni-based superalloy of the chemical composition Ni-11.7W-8.46Co-5.04Cr-4.72Al-1.05Nb-1.05Ti-0.96Mo-0.16C (wt. %). The microstructure of Ni-based superalloy consisted of γ-matrix with coherent γ'-precipitates and complex monocarbides of (Nb,Ti,W)C type. It was shown that during solidification W and Co segregated in the dendrite cores with partition ratios higher than 1, and Ni, Cr and Al segregated in the interdendritic region with partition ratios lower than 1. At a constant temperature gradient at the solid-liquid interface of 12 000 $K \cdot m^{-1}$, the measured partition ratios for Ni, W, Co, Cr, and Al depended neither on growth rate chosen from the interval $\langle 2.78 \times 10^{-6};\ 4.17 \times 10^{-5} \rangle$ $m.s^{-1}$ nor on morphology of the solid-liquid interface.

K e y w o r d s: Ni-based superalloy, directional solidification, microsegregation, partition ratio

MIKROSEGREGÁCIA V USMERNENE KRYŠTALIZOVANEJ NIKLOVEJ ŽIARUPEVNEJ ZLIATINE

V práci sme študovali štruktúru a mikrosegregáciu v usmernene kryštalizovanej niklovej žiarupevnej zliatine s chemickým zložením Ni-11,7W-8,46Co-5,04Cr-4,72Al-1,05Nb-1,05Ti-0,96Mo-0,16C (hm. %). Mikroštruktúra niklovej žiarupevnej zliatiny pozostávala z matrice γ, z koherentných precipitátov γ' a z komplexných monokarbidov typu (Nb,Ti,W)C. Na základe meraní rozdeľovacích koeficientov sme zistili, že W a Co počas kryštalizácie segregovali v primárnych osiach dendritov s rozdeľovacím koeficientom väčším ako 1 a Ni, Cr a Al v medzidendritickom priestore s rozdeľovacím koeficientom menším ako 1. Pri konštantnom teplotnom gradiente v tavenine na kryštalizačnom rozhraní 12 000 $K.m^{-1}$ namerané rozdeľovacie koeficienty Ni, W, Co, Cr a Al nezáviseli od rýchlosti rastu z intervalu $\langle 2,78 \cdot 10^{-6}; 4,17 \cdot 10^{-5} \rangle$ $m.s^{-1}$ ani od morfológie kryštalizačného rozhrania.

Ing. M. Florian, CSc., Ústav materiálov a mechaniky strojov SAV, Račianska 75, 838 12 Bratislava 38, SR.

1. Introduction

Development of directional solidification was motivated by an effort to control morphology of grain boundaries in order to improve fracture resistance. This technology was successfully applied to the production of columnar or single-crystal gas turbine blades made of superalloys or in-situ composites [1]. Directional solidification significantly improves the high temperature mechanical properties of superalloys. The solidification parameters (growth rate and temperature gradient) affect microstructural characteristics, i.e. morphology of dendrites or cells, morphology and distribution of precipitates, crystallographic texture, and microporosity. Previously published works [2, 3] on directionally solidified (DS) Ni-based superalloys showed that the temperature gradient in the melt at solid-liquid interface, G_L, and growth rate, R, directly influence primary, λ_1, and secondary, λ_2, dendrite arm spacings and dendrite tip radius.

The strength of superalloys is dependent on several factors, such as solid solution strengthening and volume fraction, morphology and size of precipitates. These factors are controlled by the chemical composition of each phase. Hence, to obtain optimal mechanical properties of Ni-based superalloys, it is required to know microsegregation processes that affect chemical composition of coexisting phases. In addition, microsegregation and macrosegregation of elements represent the main problem of processing large single crystal turbine blades (length of about 300 to 500 mm) where existing directional solidification technologies failed to prepare such components. A detail overview of possible phases that may occur in Ni-based superalloys and their effect on mechanical properties was described in detail in previously published works [4, 5].

Microsegregation represents a phenomenon attendant with dendritic solidification. Dendritic growth rate and dendrite morphology is strongly influenced by diffusion of elements in the melt in the vicinity of dendrite tip. Since a complex theoretical analysis of dendritic growth on curved solid-liquid interface is very complicated, some simplified models are used to describe the correlation between the structure and solidification parameters [5, 6].

The aim of the present work is to characterise the microstructure and to determine distribution coefficients of alloying elements in Ni-based superalloy prepared by directional solidification.

2. Experiment

Ingots of Ni-based superalloy Ni-11.7W-8.46Co-5.04Cr-4.72Al-1.05Nb-1.05Ti-0.96Mo-0.16C (wt. %) (ŽS26 alloy) with diameter of 12 mm and height of 120 mm were directionally solidified in high purity alumina crucibles in a modified Bridgman type device. The directional solidification process was described in detail by Lapin [7]. The directional solidification was performed at five growth rates

$(2.78 \times 10^{-6}; 5.55 \times 10^{-6}; 1.39 \times 10^{-5}; 2.78 \times 10^{-5}; 4.17 \times 10^{-5})$ $m \cdot s^{-1}$ and constant temperature gradient at the solid-liquid interface of 12 000 $K \cdot m^{-1}$. The temperature gradient was measured using two PtRh30-PtRh6 thermocouples by the method described by Lapin [8]. Each specimen was DS to a constant length of 60 mm and then quenched to preserve the microstructure and distribution of elements at the solid-liquid interface.

Coexisting phases were identified using transmission electron microscopy (TEM) and phase composition of the phases was determined by energy dispersive spectroscopy (EDS). TEM and EDS investigations were conducted using a JEM-100C microscope equipped with energy dispersive X-ray spectrometer KEVEX. The samples for TEM observations were thinned by mechanical grinding to a thickness of 100 μm and finally by ion milling in equipment RES 010 operated at 10 kV and current 2.5 mA. For microstructural observations by scanning electron microscopy (SEM), the samples were mechanically ground and polished using magnesium oxide suspension and then etched in a solution of 17 ml HNO_3 + 53 ml HCl + 30 ml H_2O during 2–5 s at temperature of 293 K.

Measurements of partition ratios were performed at samples from quenched solid-liquid interface by the method used by Pelachová and Lapin [9] and Lapin et al. [10] using SEM and energy dispersive spectroscopy (EDS). The concentrations of elements were measured using a line method with a line divided into 100 points. The line beginning was positioned to the middle of primary dendrite arm and line ending overreached the middle of the interdendritic region. The data of these point measurements were processed by statistical methods. Each measured value of partition ratio was estimated with its confidence interval. Outlying measurements were excluded. It was assumed the outlying measurement is that its value differs from median more than 1.5 time of interquartile range. S-curve trend analysis and polynomial smoothing were used to describe the measured data.

3. Results and discussion

Morphology of the DS alloy was cellular or dendritic containing several columnar grains (3–5) elongated in direction parallel to ingot axis [3]. Fig. 1 shows typical dendritic morphology on a cross-section of directionally solidified specimen. Fig. 2a shows typical microstructure of the alloy with all coexisting phases. As results from corresponding selected area diffraction pattern shown in Fig. 2b, the alloy contains γ-phase (nickel based solid solution), γ'-phase (intermetallic Ni_3Al phase) and a complex monocarbide (Nb, Ti, W)C. The following crystallographic orientation relationship was determined from the selected diffraction patterns:

$$(100)_{\gamma/\gamma'} \| (100)_{(Nb,Ti,W)C} : [001]_{\gamma/\gamma'} \| [001]_{(Nb,Ti,W)C} \cdot$$

Crystallographic data of all identified phases are summarised in Table 1. Face centered cubic lattices of γ/γ'-phases and carbide (Nb, Ti, W)C with a common [001] crystallographic direction are rotated with respect to each other by an angle of 6°. After directional solidification at all growth rates, the morphology of γ'--phase was cuboidal as it can be seen in Fig. 3a. Corresponding diffraction pattern from this area shown in Fig. 3b confirms the cube-cube crystallographic relationships between γ-matrix and γ'--precipitates. It should be noted that the effect of heat treatments on morphology of γ'-precipitates in single crystal ŽS26 alloy was studied in detail by Zrník et al. [11]. Another phases were not observed in the alloy that is in agreement with our preliminary calculation using PHACOMP method.

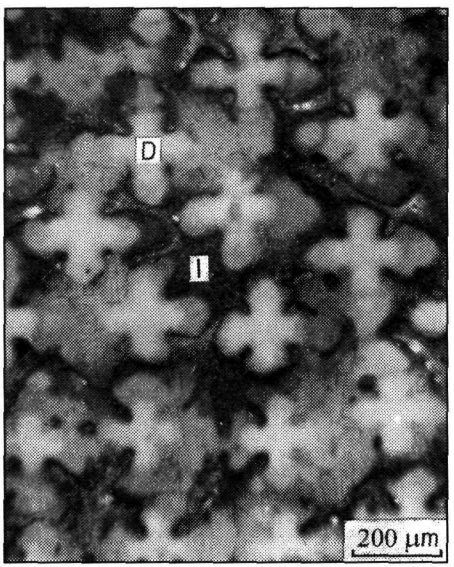

Fig. 1. Denritic structure of Ni-based superalloy. Cross-section of the ingot solidified at $R = 1.39 \times 10^{-5}$ m·s^{-1}. D – dendrite, I – interdendritic region.

Since the alloy contains 0.16 wt. % of C, carbides were observed at all growth rates. The carbides were situated in the interdendritic or intercellular regions. The same fact about positioning of MC monocarbides was published by Baldan [12]. Relatively simple carbide morphology was observed at lower growth rates. The higher the growth rate the more complex was the carbide morphology. It changed from a simple or Chinese script type, to much more complex, as illustrated in Fig. 4. Similar complex configurations were formed only at the highest growth rate of $R = 4.17 \times 10^{-5}$ m·s^{-1}. This fact is very important in connection with mechanical properties of the alloy. Leverant and Gell [13] showed that fatigue cracks nucleate from carbides and micropores in columnar as well as single crystal Mar-M200 alloy at 1266 K. This conclusion was also proved by Gabb [14] in Renè N4 alloy. On the other hand,

Table 1. Crystallographic data of identified phases

Phase	Lattice	Lattice parameter a
γ	A1	3.5238×10^{-10} m
γ'	$L1_2$	$(3.5275 - 3.5696) \times 10^{-10}$ m
(Nb, Ti, W)C	B1	$(4.4415 - 4.3365) \times 10^{-10}$ m

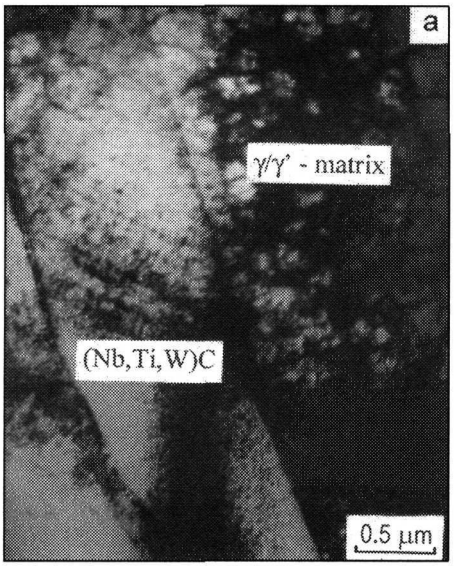

Fig. 2a. TEM micrograph of DS Ni-based superalloy.

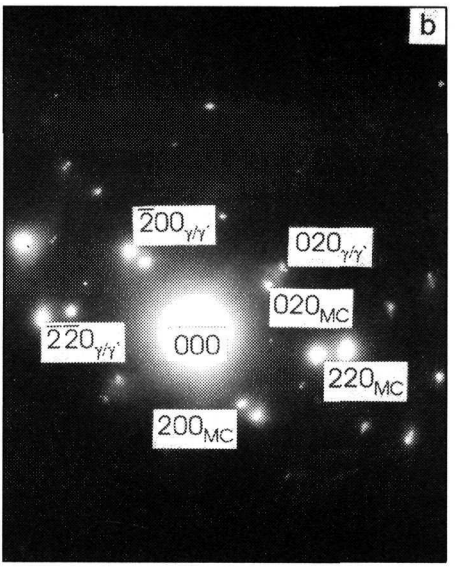

Fig. 2b. Selected area diffraction pattern corresponding to the microstructure shown in Fig. 2a.

lack of carbides can lead to poor creep properties in several directionally solidified Udimet or Nimonic types superalloys with columnar grain structure [15].

Different solutioning of alloying elements in liquid and solid causes a microsegregation phenomenon. Hence, various segregation heterogeneities that influence mechanical properties might form during solidification. In order to avoid such heterogeneities in superalloys, it is very important to identify the microsegregation mechanisms. Distribution of alloying elements between solid and liquid phases is described by a parameter that characterises isothermal-isobaric phase equilibrium in given heterogeneous system. Such parameter is partition ratio $k = C_S/C_L$ that is defined as isothermal concentration ratio of alloying element at solidus curve C_S to its concentration at liquidus curve C_L. The partition ratios of alloying elements are required to define microsegregation as well as macrosegregation processes in nickel-based superalloys.

Partition ratio measurements were performed on cross-sections prepared from mushy zone of quenched solid-liquid interfaces at various fractions of solid f_S. Fraction of solid, f_S, was determined from the following equation:

$$f_S = \frac{2 \cdot l_S}{\lambda_1}, \tag{1}$$

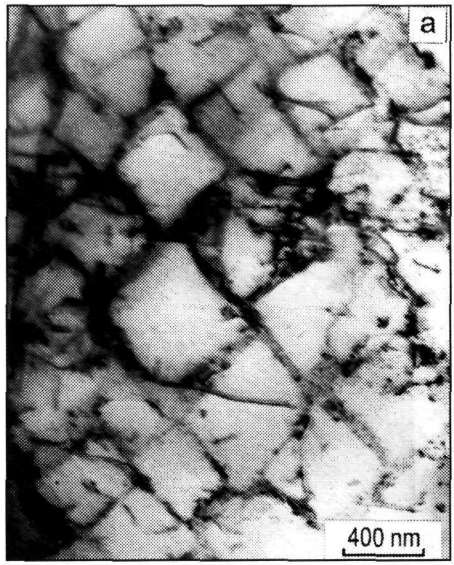

Fig. 3a. TEM micrograph of cuboidal γ' precipitates, $R = 1.39 \times 10^{-5}$ m·s^{-1}.

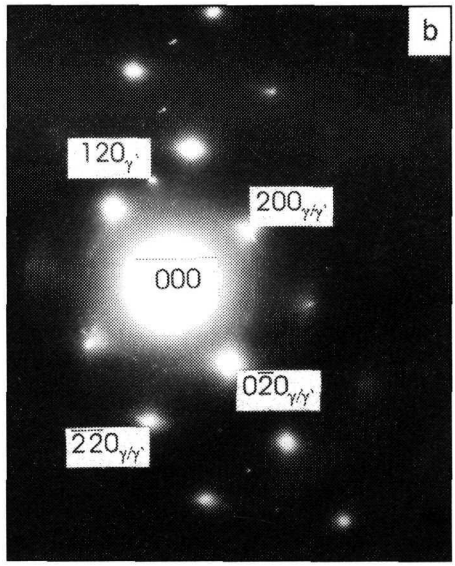

Fig. 3b. Corresponding diffraction pattern of microstructure shown in Fig. 3a.

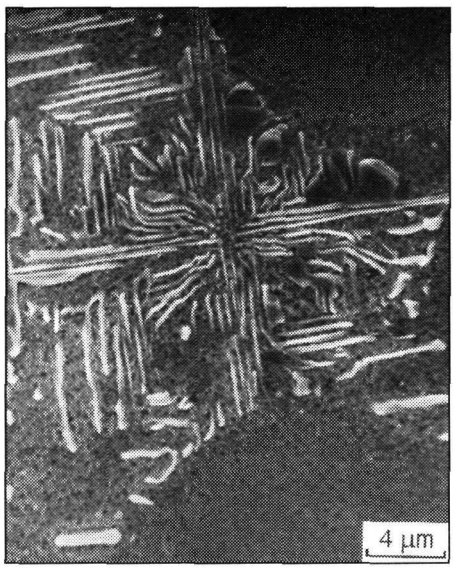

Fig. 4. Morphology and distribution of complex (Nb, Ti, W)C carbides in the interdendritic region at $R = 4.17 \times 10^{-5}$ m·s^{-1}.

where l_S is the length of secondary dendrite arms and λ_1 is the primary dendrite arms spacing. Measurements of l_S and λ_1 were previously described elsewhere [5].

Table 2. Partition ratios at various growth rates and fractions of solid

R [m·s^{-1}]	f_S	k_{Ni}	k_W	k_{Co}	k_{Al}	k_{Cr}
2.78×10^{-6}	0.7399	0.99	1.42	0.93	0.66	0.96
	0.9619	0.95	1.29	1.08	0.94	0.96
	0.9913	0.95	2.74	1.20	0.67	0.80
	1.0798	0.89	1.34	1.18	0.94	0.82
	1.2133	0.85	1.93	1.01	0.89	0.92
5.55×10^{-6}	0.7740	0.97	1.16	1.36	0.85	0.80
	0.8111	0.97	1.32	1.04	0.94	0.98
	0.8253	0.92	1.43	1.01	0.93	1.19
	0.9253	0.94	1.31	1.13	0.91	0.90
	1.3017	0.95	1.02	1.22	0.93	0.80
1.39×10^{-5}	0.4317	0.96	1.61	0.97	0.64	0.81
	0.5354	0.89	5.73	0.93	0.85	0.71
	0.7870	0.92	2.05	1.24	0.43	0.82
	0.8063	0.75	2.35	0.97	0.62	0.64
	1.0549	0.98	1.37	1.19	0.37	0.98
2.78×10^{-5}	0.5999	0.96	1.51	0.99	0.96	0.88
	0.7042	0.76	2.46	0.63	0.47	1.00
	0.7719	0.97	1.49	1.34	0.61	1.19
	0.8435	0.97	2.14	0.98	0.73	0.96
	0.9101	0.98	1.10	1.10	0.97	0.76
4.17×10^{-5}	0.2620	0.95	1.31	0.99	0.89	0.90
	0.7333	0.98	1.66	0.92	0.74	1.00
	0.7611	0.89	3.20	1.18	0.77	1.53
	0.7666	0.92	1.39	1.08	0.97	0.84
	0.8203	0.99	1.09	0.98	0.89	0.85

Fig. 5 shows distribution of elements in the mushy zone. At $f_S = 0.8111$, the concentration of elements dramatically changes, which corresponds to the solidification interface. As it can be seen from Table 2, there is practically no effect of solid fraction f_S on the partition ratios k. The same was proved by Tewari et al. [16] in PWA – 1480 Ni-based superalloy. Sellamuthu and Giamei [17] found that the partition ratios with changing solid fraction are stable for $f_S \leq 0.8$ in Mar–M200 alloy.

The calculated partition ratios are listed in Table 3. Relatively large variance of the partition ratios can be explained by highly heterogeneous microstructure of the alloy (Fig. 4). For instance, the carbides at the dendritic-interdendritic interface

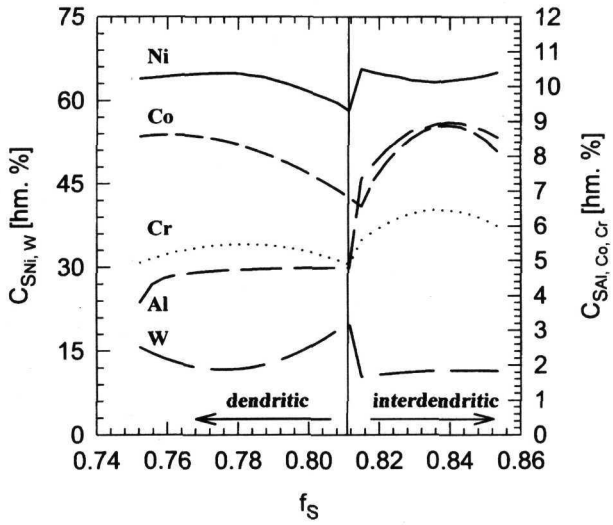

Fig. 5. Example of distribution curves measured in the mushy zone, $R = 1.39 \times 10^{-5}$ $m \cdot s^{-1}$.

Table 3. Arithmetic mean of measured partition ratios and their variance

Partition ratio	Mean	Variance
k_{Ni}	0.95 ± 0.016	0.85 – 0.99
k_W	1.59 ± 0.203	1.2 – 2.74
k_{Co}	1.08 ± 0.054	0.92 – 1.36
k_{Al}	0.78 ± 0.074	0.37 – 0.97
k_{Cr}	0.89 ± 0.056	0.64 – 1.19

might significantly affect the measured concentration profiles of elements that were used for calculations of partition ratios. It should be noted that the partition ratios of Ti and Nb were not determined in the present work due to software limitation of number of elements (max. 5 elements) that could be analysed at the same time. Table 4 summarises partition ratios in various Ni-based superalloys reported by Wills and McCartney [18]. As it can be seen from this table, the elements have the same tendency to segregate in dendrite cores and/or interdendritic regions in MAR-M002 alloy as in the studied ŽS26 alloy (Table 3). It should be added that partition ratios in other superalloys listed in Table 4 are within the interval of variance in ŽS26 alloy (Table 3).

Using one factor analysis of variance, it was found that there is no effect of the

Table 4. Measured values of partition ratios in various alloys [17]

Partition ratio	RR2000	RR2060	SRR99	MAR-M002
k_{Al}	0.97	0.95	1.00	0.99
k_{Co}	1.08	1.10	1.09	1.16
k_{Cr}	1.10	1.06	0.95	0.95
k_{Hf}	–	–	–	0.06
k_{Mo}	0.97	0.91	–	–
k_{Ti}	0.60	0.65	0.68	0.60
k_{Ta}	–	0.58	0.52	0.45
k_{W}	–	0.81	1.06	1.12
k_{V}	1.13	–	–	–

growth rates and morphology of the solid-liquid interface on the partition ratios values.

4. Conclusions

On the base of studying the microstructure and partition ratios in directionally solidified Ni-based superalloy the following conclusions were reached:

1. The microstructure of the analysed Ni-based superalloy consisted of γ--matrix and coherent cuboidal γ'-precipitates. Complex monocarbides of (Nb, Ti, W)C type were formed in the interdendritic regions. Cubic lattices of γ/γ'--phases and (Nb, Ti, W)C carbide with a common [001] crystallographic direction were rotated with respect to each other by an angle of 6°.

2. During solidification W and Co segregated in the dendrite cores with partition ratios higher than 1 and Ni, Cr and Al segregated in the interdendritic region with partition ratios lower than 1.

3. The measured partition ratios for Ni, W, Co, Cr, and Al did not depend on growth rate and morphology of the solid-liquid interface over the studied growth rate interval $\langle 2.78 \times 10^{-6}; 4.17 \times 10^{-5} \rangle$ m.s^{-1}.

Acknowledgements

This work was supported by Scientific Grant Agency of Ministry of Education of the Slovak Republic and Slovak Academy of Sciences under the contract VEGA 5091/98.

REFERENCES

[1] LAPIN, J.—IVAN, J.: Scripta Metall. Mater., *33*, 1995, p. 391.
[2] LAPIN, J.—KLIMOVÁ, A.—VELÍSEK, R.—KURSA, M.: Scripta Mater., *37*, 1997, p. 85.
[3] FLORIAN, M.—KOVÁČOVÁ, K.: Kovove Mater., *31*, 1993, p. 506.

[4] ŽITŇANSKÝ, M.: Fyzikálno-metalurgické aspekty procesu riadenej kryštalizácie žiarupevných niklových zliatin a rafinácie. [Doctor Thesis]. Strojnícka fakulta SVŠT, Bratislava 1984.
[5] FLORIAN, M.: Fyzikálno-metalurgické parametre žiarupevnej zliatiny na báze Ni pripravenej usmernenou kryštalizáciou. [PhD. Thesis]. Ústav materiálov a mechaniky strojov SAV, Bratislava 1994.
[6] GIOVANOLA, B.—KURZ, W.: Z. Metallkd., *82*, 1991, p. 83.
[7] LAPIN, J.: Kovove Mater., *34*, 1996, p. 265.
[8] LAPIN, J.: Štúdium kontinuálnej zmeny rastových parametrov eutektických zložených materiálov. [PhD Thesis]. Ústav materiálov a mechaniky strojov SAV, Bratislava 1991.
[9] PELACHOVÁ, T.—LAPIN, J.: Kovove Mater., *37*, 1999, 6, p. 399.
[10] LAPIN, J.—WIERZBINSKI, S.—PELACHOVÁ, T.: Intermetallics, *7*, 1999, p. 705.
[11] ZRNÍK, J.—ŽITŇANSKÝ, M.—HAZLINGER, M.: Kovove Mater., *37*, 1999, p. 246.
[12] BALDAN, A.: J. Mater. Sci., *26*, 1991, p. 3879.
[13] LEVERANT, G. R.—GELL, M.: Trans. Metallurg. Soc. AIME, *245*, 1969, p. 1167.
[14] GABB, T. P.—GAYDA, J.—MINER, R.: Metallurg. Trans., *17A*, 1986, 3, p. 497.
[15] DECKER, R. F.—SIMS, C. T.: The Metallurgy of Nickel – Base Alloys. In: The Superalloys. Eds.: Sims, C. T., Hagel, W. C. John Wiley and Sons, New York 1972, p. 33.
[16] TEWARI, S. N. et al.: Mat. Sci. Eng. A, *A141*, 1991, p. 97.
[17] SELLAMUTHU, R.—GIAMEI, A. F.: Metall. Trans. A, *17A*, 1986, p. 419.
[18] WILLS, V. A.—McCARTNEY, D. G.: Mat. Sci. Eng. A, *A145*, 1991, p. 223.

Received: 16.2.2000